Brief Report

Novel insights into the taxonomic diversity and molecular mechanisms of bacterial Mn(III) reduction

Nadia Szeinbaum, [1,2,3] Brook L. Nunn, [4]
Amanda R. Cavazos, [2] Sean A. Crowe, [2,5,6]
Frank J. Stewart, [1,7] Thomas J. DiChristina, [1]
Christopher T. Reinhard [2,3] and
Jennifer B. Glass [2,3†*]

[1] School of Biological Sciences, Georgia Institute of Technology, Atlanta, GA, USA.
[2] School of Earth and Atmospheric Sciences, Georgia Institute of Technology, Atlanta, GA, USA.
[3] NASA Astrobiology Institute, Alternative Earths Team, Mountain View, CA, USA.
[4] Department of Genome Sciences, University of Washington, Seattle, WA, USA.
[5] Department of Microbiology and Immunology, University of British Columbia, Vancouver, BC, Canada.
[6] Department of Earth, Ocean, and Atmospheric Sciences, University of British Columbia, Vancouver, BC, Canada.
[7] Department of Microbiology and Immunology, Montana State University, Bozeman, MT, USA.

Summary

Soluble ligand-bound Mn(III) can support anaerobic microbial respiration in diverse aquatic environments. Thus far, Mn(III) reduction has only been associated with certain *Gammaproteobacteria*. Here, we characterized microbial communities enriched from Mn-replete sediments of Lake Matano, Indonesia. Our results provide the first evidence for the biological reduction of soluble Mn(III) outside the *Gammaproteobacteria*. Metagenome assembly and binning revealed a novel betaproteobacterium, which we designate 'Candidatus Dechloromonas occultata.' This organism dominated the enrichment and expressed a porin-cytochrome *c* complex typically associated with iron-oxidizing *Betaproteobacteria* and a novel cytochrome c-rich protein cluster (Occ), including an undecaheme putatively involved in extracellular electron transfer. This *occ* gene cluster was also detected in diverse aquatic bacteria, including uncultivated *Betaproteobacteria* from the deep subsurface. These observations provide new insight into the taxonomic and functional diversity of microbially driven Mn(III) reduction in natural environments.

Introduction

Manganese(III) is a strong oxidant with a reduction potential close to molecular oxygen (Kostka *et al*., 1995). Mn(III) is short-lived and unstable, but its stability is greatly increased when bound to ligands (Luther III *et al*., 2015). Ligand-bound Mn(III) is often the most abundant dissolved Mn species in sediment pore waters (Madison *et al*., 2013; Oldham *et al*., 2019) and soils (Heintze and Mann, 1947), with the potential to facilitate one-electron redox reactions in a variety of biogeochemical cycles (Luther III *et al*., 2015). Microbes accelerate the oxidation and reduction of Mn by orders of magnitude compared with abiotic mechanisms (Hem, 1963; Diem and Stumm, 1984; Morgan, 2005; Tebo *et al*., 2005; Learman *et al*., 2011; Luther *et al*., 2018; Jung *et al*., 2020; Yu and Leadbetter 2020). Yet, despite clear evidence for the environmental importance of Mn(III), knowledge about microbial Mn(III) cycling pathways remains fragmented.

To date, only *Shewanella* spp. (*Gammaproteobacteria*) have been confirmed to respire soluble Mn(III) (Kostka *et al*., 1995; Szeinbaum *et al*., 2014). *Shewanella* respire Mn(III) using the Mtr pathway (Szeinbaum *et al*., 2017), a porin-cytochrome (PCC) conduit that transports electrons across the periplasm for extracellular respiration of Mn(III/IV), Fe(III) and other metals (Richardson *et al*., 2012; Shi *et al*., 2016). Many Fe(II)-oxidizing *Betaproteobacteria* also contain PCCs (MtoAB, generally lacking the C subunit), which are proposed to oxidize Fe(II) to Fe(III) by running the PCC in reverse (Emerson *et al*., 2013; Kato *et al*., 2015; He *et al*., 2017). In some metal-reducing *Gammaproteobacteria* and *Deltaproteobacteria*, extracellular undecaheme (11-heme) UndA is thought to play a key functional role in

soluble Fe(III) reduction (Fredrickson *et al.*, 2008; Shi *et al.*, 2011; Smith *et al.*, 2013; Yang *et al.*, 2013). UndA's crystal structure shows a surface-exposed heme surrounded by positive charges, which may bind negatively charged soluble iron chelates (Edwards *et al.*, 2012). Environmental omics suggest that metal reduction by *Betaproteobacteria* may be widespread in the deep subsurface (Anantharaman *et al.*, 2016; Hernsdorf *et al.*, 2017). However, only a few Fe(III)-reducing *Betaproteobacteria* isolates have been characterized to date (Cummings *et al.*, 1999; Finneran *et al.*, 2003), and little is known about metal reduction pathways in *Betaproteobacteria*.

Manganese reduction coupled to methane (CH_4) oxidation is a novel metabolism only recently discovered in cultures enriched in Archaea (Ettwig *et al.*, 2016; Leu *et al.*, 2020). Biological and geochemical evidence suggest that this metabolism may be found in a variety of environments (Beal *et al.*, 2009; Crowe *et al.*, 2011; Riedinger *et al.*, 2014), including Fe-rich Lake Matano, Indonesia. In an attempt to explore whether CH_4 can fuel microbial Mn(III) reduction in enrichments inoculated with sediments from Lake Matano, Indonesia, which has active and pronounced microbial Mn and CH_4 cycles (Jones *et al.*, 2011), we uncovered a novel betaproteobacterium as the most dominant and active member of our Mn(III)-reducing enrichment culture. Our results provide the first evidence for the biological reduction of soluble Mn(III) outside *Gammaproteobacteria* and provide evidence for a new biochemical pathway involved in extracellular electron transfer.

Results and discussion

Enrichment of Mn(III)-reducing populations

Lake Matano, Indonesia, is a permanently stratified ultra-oligotrophic lake (Crowe *et al.*, 2008). Below its oxic surface waters, Lake Matano's permanently anoxic and stratified waters are highly enriched in iron and manganese, and support the activity of Mn cycling organisms with organic carbon and CH_4 as potential sources of electrons (Crowe *et al.*, 2011; Jones *et al.*, 2011; Kuntz *et al.*, 2015; Sturm *et al.*, 2019). We designed an enrichment strategy to select for microbes capable of anaerobic CH_4 oxidation coupled to soluble Mn(III) reduction by incubating anoxic Lake Matano sediment communities with soluble Mn(III)-pyrophosphate as the electron acceptor (with 2% O_2 in a subset of bottles), and CH_4 as the sole electron donor and carbon source after pre-incubation to deplete endogenous organic carbon (see Supporting Information for enrichment details). Enrichment cultures were transferred into fresh media after Mn(III) was completely reduced to Mn(II), for a total of five transfers over 395 days. By the fourth transfer, cultures with CH_4 headspace (with or without 2% O_2)
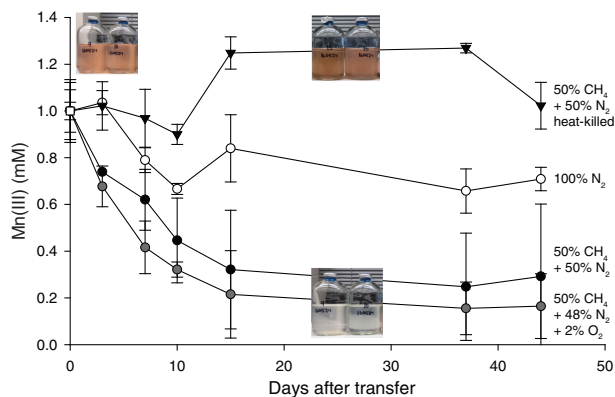

Fig. 1. Consumption of Mn(III) in Lake Matano enrichments in the presence and absence of methane. Sediment-free cultures (transfer 4), from 335 days after the initial enrichment, were incubated for 45 days with 1 mM Mn(III) pyrophosphate as the sole electron acceptor. One set was incubated with Mn(III) and 2% O_2. Initial bottle headspace contained 50% CH_4 + 50% N_2 (black circles), 50% CH_4 + 48% N_2 + 2% O_2 (grey circles), 100% N_2 (white circles) and 50% CH_4 + 50% N_2 heat-killed controls (black triangles). Error bars are standard deviations from duplicate experiments. Colour change from red to clear indicates Mn(III) reduction.

reduced ~80% of soluble Mn(III) compared with ~30% with N_2 headspace (Fig. 1). 16S rRNA gene sequences were dominated by *Betaproteobacteria* (*Rhodocyclales*; 8%–35%) and *Deltaproteobacteria* (*Desulfuromonadales*; 13%–26%; Fig. S1). $^{13}CH_4$ oxidation to $^{13}CO_2$ was undetectable (Fig. S2).

Samples for metagenomic and metaproteomic analysis were harvested from the fifth transfer (Fig. S1). Out of 2952 proteins identified in the proteome, 90% were assigned to *Betaproteobacteria*; of those, 72% mapped to a 99.5% complete metagenome-assembled genome (MAG; *Rhodocyclales* bacterium GT-UBC; NCBI accession QXPY01000000) with 81%–82% average nucleotide identity and phylogenetic affiliation to *Dechloromonas* spp. (Table S1; Fig. S3). This MAG is named here '*Candidatus* Dechloromonas occultata' sp. nov.; etymology: occultata; (L. fem. adj. 'hidden'). The remaining 10% of proteins mapped to *Deltaproteobacteria*; of those, 70% mapped to a nearly complete MAG (*Desulfuromonadales* bacterium GT-UBC; NCBI accession RHLS01000000) with 80% ANI to *Geobacter sulfurreducens*. This MAG is named here '*Candidatus* Geobacter occultata'.

Cytochrome expression during Mn(III) reduction

Cytochromes containing multiple *c*-type hemes are key for electron transport during microbial metal transformations, and therefore also expected to play a role in Mn(III) reduction. Numerous mono-, di-, and multi (>3)-heme cytochromes (MHCs) were expressed by '*Ca*. D. occultata' in Mn(III)-reducing cultures. Nine out of 15 MHCs encoded by the '*Ca*. D. occultata' MAG were

expressed, including two decahemes similar to MtoA in Fe(II)-oxidizing *Betaproteobacteria* (Tables 1, Tables S2, S3; Fig. 2A, Fig. S4). Several highly expressed MHCs were encoded on a previously unreported 19-gene cluster with 10 cytochrome-*c* proteins, hereafter *occA-S* (Table 1; Fig. 2B, Figs S5 and S6). OccP was predicted to be an extracellular undecaheme protein of ~100 kDa (922 amino acids). '*Ca.* Dechloromonas occultata' may reduce Mn(III) using the novel extracellular undecaheme OccP as the terminal Mn(III) reductase. Experimental verification of the function of the putative Occ complex is currently limited by the scarcity of genetically tractable *Betaproteobacteria*.

Proteins with 40%–60% identity to the expressed '*Ca.* D. occultata' OccP protein were widely distributed in *Betaproteobacteria* from diverse freshwaters and deep subsurface groundwaters, as well as in several *Gammaproteobacteria* and one alphaproteobacterium (Fig. 2D; Table S3). Most *occP*-containing bacteria also possessed *mtoA* and denitrification genes (Fig. 2D; Fig. S7). These results widen the phylogenetic diversity of candidate extracellular MHCs that may be involved in microbial Mn(III) reduction.

Heme-copper oxidases in '*Ca. D. occultata*'

'*Ca.* D. occultata' expressed high-affinity cbb_3-type cytochrome *c* oxidase (CcoNOQP) associated with microaerobic respiration (Table S4). Features of the '*Ca.* D. occultata' *occS* gene product, including conserved histidine residues (H-94, H-411 and H-413) that bind hemes a and a_3, as well as the H-276 residue that binds Cu_B (Fig. S6), suggest that OccS may function similarly to CcoN, the terminal heme-copper oxidase proton pump in aerobic respiration. All identified OccS amino acid sequences lack Cu_B ligands Y-280 and H-403, and most lack Cu_B ligands H-325 and H-326. OccS sequences also lack polar and ionizable amino acids that comprise the well-studied D and K channels involved in proton translocation in characterized cytochrome *c* oxidases (Blomberg and Siegbahn, 2014), but contain conserved H, C, E, D and Y residues that may serve in alternate proton translocation pathways, similar to those recently discovered in qNOR (Gonska et al., 2018). OccS homologues were also found in *Azoarcus* spp. and deep subsurface *Betaproteobacteria* (Fig. S6).

Expression of denitrification proteins and possible sources of oxidized nitrogen species

Periplasmic nitrate reductase (NapA), cytochrome nitrite reductase (NirS) and type II atypical nitrous oxide reductase (cNosZ; Fig. S7) were highly expressed by '*Ca.* D. occultata' (Table 1). Expression of the denitrification pathway was not expected because oxidized nitrogen species were not added to the medium, to which the only nitrogen supplied was 0.2 mM NH_4Cl (along with headspace N_2). Oxidized nitrogen species could result from the oxidation of NH_4Cl, but we did not find any of the canonical genes for aerobic nor anaerobic ammonia oxidation, nor did we measure any ammonium oxidation in experimental bottles from the transfer used to make Fig. 1.

The expression of denitrification genes is controlled by a diverse array of transcriptional regulators that depend on different signals including low levels of oxygen, even in the absence of nitrate (Spiro, 2012; Lin et al., 2018). The close redox potential of Mn(III)-pyrophosphate (~0.8 V; Yamaguchi and Sawyer, 1985) to oxidized nitrogen species (0.35–0.75 V) at circumneutral pH and the lack of oxygen in the media could have induced the expression of denitrification genes simultaneously with Mn(III)-reduction genes. *Gammaproteobacteria*, for example, reduce Mn(III) even in the presence of nitrate (Kostka et al., 1995), and there is precedent for microbial use of multiple electron acceptors, e.g. 'co-respiration' of oxygen and nitrate during aerobic denitrification (Chen and Strous, 2013; Ji et al., 2015).

Because solid-phase Mn(III) is known to chemically oxidize NH_4^+ (Aigle et al., 2017; Boumaiza et al., 2018), we tested for abiotic NH_4^+ oxidation by soluble Mn(III) (1 mM). Ammonium concentrations remained unchanged, and no N_2O or NO_x^- production was observed (Fig. S8), likely because our experiments lacked solid surfaces to mediate electron transfer. Similarly, N_2O levels in the headspace of our experimental bottles with Mn(III)-reducing cultures were near or below the detection limit (data not shown). These findings are consistent with the lack of detectable ammonium oxidation by Mn(III) pyrophosphate in estuarine sediments (Crowe et al., 2012).

Electron donors

Methane was the only electron donor added intentionally to the enrichment cultures, to select for organisms that oxidize methane anaerobically. Yet, we did not detect $^{13}CO_2$ after the addition of $^{13}CH_4$ (Fig. S2). One explanation is that $^{13}CO_2$ was produced, but was subsequently assimilated by other members of the microbial community such as abundant Deltaproteobacteria (Fig. S1), as observed in previous studies (Wegener et al., 2008). A filtration step included in our protocol to measure $^{13}CO_2$ would have excluded ^{13}C-enriched biomass from our analyses. Alternatively, we considered other electron donors that might have been unintentionally present in trace amounts, but sufficiently abundant to drive the observed ~300–600 μM Mn(III) reduction (Fig. 1). The ethanol catabolism pathway (PQQ-dependent methanol/ethanol dehydrogenase (RIX45050), quinoprotein alcohol dehydrogenase

Table 1. Expression levels for select '*Ca.* Dechloromonas occultata' and '*Ca.* Geobacter occultata' proteins in the presence of CH_4 and N_2.

Enzyme complex/category	Function	Protein sequence predictions		Motifs				Normalized peptide abundance						
								By treatment				Differential peptide		
		Proteins	NCBI ID	SP	TMH	CxxCH	P-sort	CH_4	SD	N_2	SD	Avg	SD	*p*-value
Ca. Dechloromonas occultata														
Mto-1	Outer membrane porin-cytochrome c electron conduit	MtoX-1 (cyt-b)	RIX49676	N	5	0	IM	2.7	0.5	3.6	0.2	0.8	0.2	0.2
		MtoY-1 (MCP)	RIX49677	N	2	1	IM	10	2	15	2	0.6	0.1	0.004
		MtoB-1 (porin)	RIX49678	Y	0	0	OM							
	conduit	MtoA-1	RIX49874	Y	1	10	P	5	1	2.5	0.1	1.9	0.4	0.1
		MtoD-1	RIX49875	N	0	1	P							
Mto-2	Outer membrane porin-cytochrome c electron conduit	MtoX-2 (cyt-b)	RIX48942	N	4	0	IM							
		MtoB-2 (porin)	RIX48943	Y	0	0	OM	8	1	16	0.2	0.5	0.1	0.04
	conduit	MtoA-2	RIX48944	Y	1	10	P	7.3	0.8	4	2	2.1	1.3	0.2
		MtoD-2	**RIX48945**	**Y**	**1**	**1**	**U**	**2.6**	**0.3**	**0.7**	**0.3**	**4.0**	**1.4**	**0.003**
Occ	Membrane-spanning electron transport cytochromes	**OccA**	**RIX49688**	**Y**	**1**	**3**	**P**	**4**	**0.5**	**0.7**	**0.6**	**7.8**	**5.7**	**0.01**
		OccB	**RIX49689**	**Y**	**0**	**3**	**U**	**41**	**4**	**19**	**2**	**2.2**	**0.0**	**0.03**
		OccC	RIX49877	N	0	1	U							
		OccD	RIX49878	N	0	3	U							
		OccE (6-NHL)	RIX49690	N	1	0	U	22	2.1	20.5	0.2	1.1	0.1	0.2
		OccF	RIX49691	Y	2	4	E	13	0.7	10.1	0.1	1.3	0.1	0.06
		OccG (PPIase)	**RIX49692**	**N**	**0**	**0**	**U**	**14**	**1**	**3.3**	**0.5**	**4.2**	**0.3**	**0.01**
		OccH	RIX49693	N	0	0	OM/E	6.0	0.2	7.7	0.6	0.8	0.1	0.10
		OccI	RIX49694	N	1	3	U	7	2.5	2.3	0.0	2.9	1.1	0.1
		OccJ	**RIX49879**	**Y**	**0**	**4**	**U**	**44**	**0.2**	**19**	**3**	**2.4**	**0.4**	**0.03**
		OccK	**RIX49880**	**N**	**0**	**0**	**C**	**39**	**6**	**13**	**1**	**3.0**	**0.2**	**0.04**
		OccL	RIX49695	N	1	3	U							
		OccM	RIX49881	N	2	0	U							
		OccN (6 NHL)	RIX49696	N	0	0	U	5.7	0.3	6	1	0.9	0.1	0.2
		OccO (6 NHL)	RIX49882	N	0	0	U	1.2	0.8	4.2	0.4	0.3	0.2	0.03
		OccP	RIX49697	N	0	11	E	14	2	12	3	1.2	0.5	0.4
		OccQ	RIX49698	Y	4	0	IM							
		OccR	RIX49883	N	8	0	IM							
		OccS	RIX49699	N	12	0	IM							
Cyt c	Mono- and di-heme c-type cytochromes involved in electron transfer	**Cyt c5**	**RIX47670**	**N**	**1**	**1**	**U**	**27**	**2**	**9**	**3**	**3.2**	**0.8**	**0.01**
		Cyt c5	RIX40984	Y	1	2	P	19	2	6	1	3.3	1.0	0.06
		Cyt c/C_2	RIX44710	Y	1	1	P	17	5	3.6	0.8	4.8	2.3	0.09
		Cyt c/C_2	RIX49630	Y	1	1	P	7	1	1.2	0.9	8.2	6.6	0.07
		Cyt c551/c552	RIX49087	Y	0	1	P	13	3	2.8	0.0	4.8	1.1	0.06
		Cyt c4	RIX48804	Y	0	2	P	16	0.8	9.8	0.8	1.6	0.2	0.06
		Cyt c4	RIX44782	Y	0	2	P	4	2	1.7	0.7	2.6	0.1	0.08
		Cyt c4	**RIX45018**	**Y**	**0**	**2**	**P**	**7**	**0.6**	**2.2**	**0.2**	**3.0**	**0.0**	**0.02**
Nap	Periplasmic nitrate reductase	NapA	RIX41011	Y	0	0	P	76	2	67	3	1.1	0.1	0.1
		NapB	**RIX41010**	**Y**	**1**	**2**	**P**	**15**	**1**	**5**	**2**	**3.2**	**0.9**	**0.02**
		NapC	RIX41009	N	1	4	IM	12	3	13	1	1.0	0.2	0.1
Nir	Nitrite reductase	NirS	RIX44719	Y	0	1	P	58	2	44	4	1.3	0.2	0.1
		NirB	RIX44720	Y	1	2	P	14	3	10	2	1.5	0.6	0.2
		NirC	RIX44788	N	0	1	P							
		NirF	RIX44721	Y	1	0	P or C	2	1	7	1	0.3	0.1	0.02

Category	Protein	Gene	Locus tag				Loc	3.5	0.7	3.2	0.7	1.1	0.0	0.1
Nor	Nitric oxide reductase	NorC	RIX45182	N	1	1	IM	77	17	66	8	1.2	0.3	0.2
		NorB	RIX45183	N	12	1	IM	16	2	4	2	4.9	3.3	0.08
cNos	Type II nitrous oxide reductase	cNosZ	RIX42539	Y	0	0	P							
		cNosC1	RIX42538	Y	1	1	P							
		cNosC2	**RIX42537**	**Y**	**1**	**2**	**P**	**10**	**0.1**	**3.9**	**0.3**	**2.6**	**0.1**	**0.02**
		cNosB	RIX42536	N	6	0	IM							
		cNosD	RIX42535	N	0	0	P							
		cNosG	RIX42534	N	1	0	C							
		cNosH	RIX42533	N	4	0	IM							
Qcr	Menaquinol-cytochrome c reductase complex	QcrA	RIX41976	N	9	0	CM							
		QcrB	RIX41977	N	9	0	CM							
		QcrC	RIX41978	N	1	0	CM							
Proteases	Serine protease		**RIX49468**	**N**	**0**	**0**	**P**	**27**	**2**	**1.0**	**0.3**	**29.0**	**9.9**	**0.02**
	Carboxyl-terminal protease (S41)		**RIX48818**	**N**	**1**	**0**	**CM**	**18.5**	**0.8**	**8.0**	**0.9**	**2.3**	**0.1**	**0.0002**
	DUF4214 protein		**RIX44180**	**N**	**0**	**0**	**OM/E**	**146**	**25**	**43**	**0.6**	**3.4**	**0.5**	**0.05**
Membrane/Extracellular	S-layer protein		RIX44181	N	0	0	U	8	0.5	10	0.6	0.8	0.1	0.14
	PEP-CTERM sorting protein		**RIX45463**	**Y**	**1**	**0**	**E**	**68**	**6**	**33**	**10**	**2.1**	**0.5**	**0.03**
	Tol-Pal system protein	TolB	**RIX44015**	**Y**	**0**	**0**	**P**	**20**	**2**	**12**	**1**	**1.7**	**0.0**	**0.03**
	Peptidoglycan-associated lipoprotein	Pal	**RIX44016**	**N**	**0**	**0**	**OM**	**27.3**	**0.2**	**10**	**3**	**2.7**	**0.7**	**0.04**
	Tol-Pal system protein	YbgF	RIX44017	Y	0	0	U	10.8	0.4	4	2	3.7	2.2	0.06
	Pilus assembly protein		**RIX46961**	**N**	**0**	**0**	**U**	**54**	**5**	**30**	**5**	**1.8**	**0.1**	**0.001**
Other	Ethanol/methanol dehydrogenase		**RIX45050**	**Y**	**0**	**0**	**P**	**37**	**4**	**17**	**1**	**2.2**	**0.1**	**0.03**
	Alcohol dehydrogenase		RIX45053	Y	0	0	P	12.4	1.4	14.2	1.7	0.9	0.0	0.04
	Aldehyde dehydrogenase		RIX45061	Y	0	0	P	125	31	221	75	0.6	0.1	0.10
	Phasin family granule-associated protein		**RIX40682**	**N**	**0**	**0**	**U**	**49**	**2**	**22**	**1**	**2.2**	**0.2**	**0.03**
	Phasin family granule-associated protein		**RIX40683**	**Y**	**0**	**0**	**U**	**34**	**4**	**16**	**1**	**2.1**	**0.0**	**0.03**
	High potential iron-sulfur protein		**RIX49681**	**Y**	**0**	**0**	**U**	**10.79**	**0.01**	**6.5**	**0.4**	**1.7**	**0.1**	**0.02**
	Electron transfer flavoprotein	FixA	**RIX43544**	**N**	**0**	**0**	**C**	**16**	**3**	**10**	**2**	**1.7**	**0.0**	**0.04**
	NAD-reducing hydrogenase	HoxH	RIX46736	N	0	0	C	22.9	0.7	37	3	0.6	0.1	0.07

(Continues)

Table 1. Continued

Enzyme complex/category	Protein sequence predictions							Normalized peptide abundance						
				Motifs				By treatment				Differential peptide		
	Function	Proteins	NCBI ID	SP	TMH	CxxCH	P-sort	CH_4	SD	N_2	SD	Avg	SD	p-value
Ca. Geobacter occultata														
Hydrogenase	[Ni/Fe] hydrogenase, group 1, small subunit	HyaA	RNC64339	Y	0	0	P	11.1	0.4	3	1	5	2	0.06
	[Ni/Fe] hydrogenase, group 1, large subunit	**HyaB**	**RNC64340**	N	0	0	**P**	**32**	**0**	**11**	**5**	**3**	**1**	**0.01**
E-pilus	Type IV pilin	PilA	RNC67631	N	1	0	E	93	3	18	3	5.6	0.6	0.02

Grey boxes indicate membrane proteins. SP: signal peptide (Y: present/N: absent); TMH: numbers of transmembrane helices; CxxCH: number of heme-binding motifs; P-sort: predicted cellular location based on Psort v.3.0. MCP: methyl-accepting chemotaxis protein; PPIase: Peptidyl-proline isomerase; P: periplasm; C: cytoplasm; OM: outer membrane; IM: inner membrane, E: extracellular; U: unknown. MtoX and MtoY were predicted to be an inner membrane cytochrome-b protein and a methyl-accepting chemotaxis protein respectively. Membrane proteins may be under-represented by mass spectrometry-based metaproteomic analyses, which inherently favour soluble over insoluble membrane-bound or hydrophobic proteins. Bold proteins indicate proteins that were significantly more expressed with CH_4 than N_2 ($CH_4/N_2 > 1$; $p < 0.05$). p values indicate significance of abundance difference between CH_4 and N_2 treatments.

(RIX45053) and an NAD$^+$-dependent aldehyde dehydrogenase-II (RIX45061)) were all highly expressed in 'Ca. *D. occultata*' (Table 1). Ethanol could have been introduced to the bottles during culture preparation during sterilization of bottle stoppers. Based on the stoichiometry of ethanol oxidation coupled to Mn(III) reduction:

$$2CH_3CH_2OH + 10H_2O + 5Mn(III)_2(P_2O_7)_3$$
$$\rightarrow 4HCO_3^- + 10Mn^{2+} + 24H^+ + 15(P_2O_7)^{2-}$$
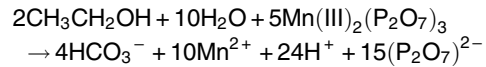
One-hundred and fifty micromolar ethanol would be required to reduce 600 µM of Mn(III), which equates to ~1 µl of 70% ethanol (12 M) into 100 ml culture medium. We conclude that trace contamination of ethanol was likely the major electron donor to our cultures.

It is also possible that other substrates, such as H_2 from fermentation by other microbes in the enrichment or from impurities in the headspace gas, could have supplied another source of electrons. Indeed, an NAD-reducing hydrogenase (RIX44099-100) was expressed by 'Ca. D. occultata' (Table 1). Based on the stoichiometry of H_2 oxidation coupled to Mn(III) reduction:

$$H_2 + Mn(III)_2(P_2O_7)_3 \rightarrow 2H^+ + 2Mn^{2+} + 3(P_2O_7)^{2-}$$
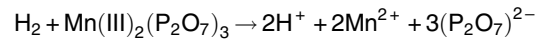
Six hundred micromolar H_2 would be required to reduce 600 µM of Mn(III). Thus, H_2 may have contributed electrons to Mn(III) reduction but is not likely sole electron donor. A combination of ethanol, H_2 and other trace contaminants would likely have been necessary to provide enough electrons for the additional reduction of Mn(III) observed in the $^{13}CH_4$-amended cultures compared with the controls lacking $^{13}CH_4$. There is precedent for other metal-reducers simultaneously using H_2 and an organic electron donor (Brown *et al*., 2005).

Another trace source of organics to our cultures could have been leaching from the rubber stoppers, which were black bromobutyl and pre-boiled in 0.1 N NaOH. A previous study reported that organics leaked an array of n-alkanes (C_{16}–C_{34}) and unidentified organic contaminants in black bromobutyl stoppers (Niemann *et al*., 2015). It is also conceivable that trace organic was introduced as impurities in solid Mn(III) oxide powder (99% purity) used to synthesize Mn(III)-pyrophosphate.

Finally, we considered the possibility that 0.2 mM NH_4^+, added to the cultures as a nitrogen source, could have provided the electron donor, via an unknown pathway. Based on the stoichiometry of NH_4^+ oxidation coupled to Mn(III) reduction:

$$NH_4^+ + 3H_2O + 4Mn(III)_2(P_2O_7)_3$$
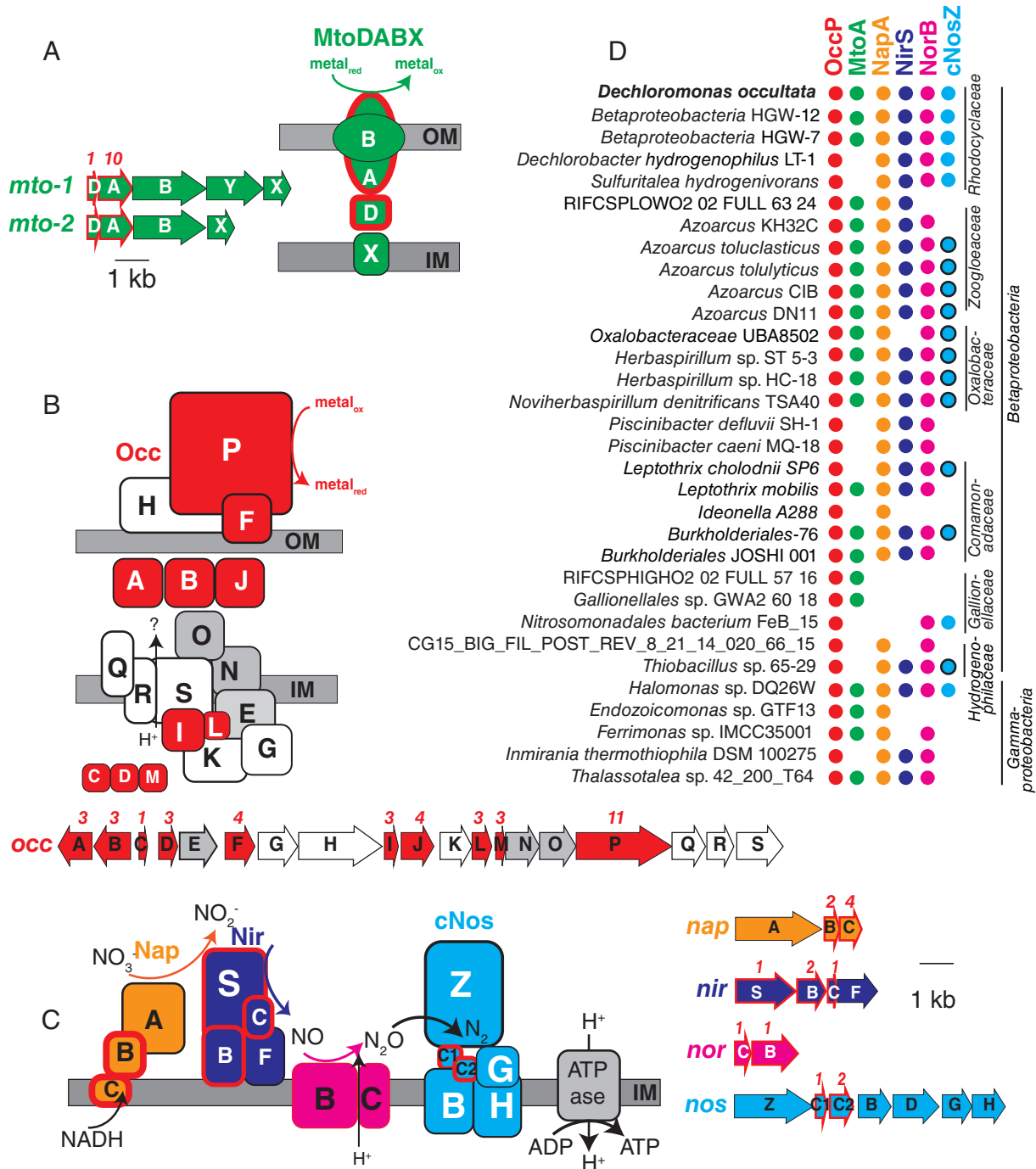$$\rightarrow NO_3^- + 8H^+ + 8Mn^{2+} + 4(P_2O_7)^{2-}$$
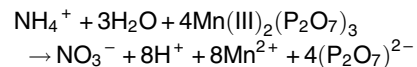
Fig. 2. Gene arrangement, predicted protein location and taxonomic distribution of major expressed respiratory complexes in '*Ca*. D. occultata'. A: MtoDAB(Y)X porin-cytochrome *c* electron conduit; B: OccA-S; C: denitrification complexes (Nap, Nir, Nor and cNos); D: Occurrence of key marker genes in *Betaproteobacteria* and *Gammaproteobacteria* with >95% complete genomes that encode OccP. Protein sequences from '*Ca*. D. occultata' were used as a query against a genome database and searched using PSI BLAST. Matches with identities >40%, query coverage >80% and *E* values <10^{-5} were considered positive. Red fill around genes and proteins indicate cytochrome-*c* proteins. Black outlines around blue circles in D indicate type I nitrous oxide reductase to distinguish from blue dots (type II/cytochrome-nitrous oxide reductase). Grey-shaded genes on the *occ* gene cluster indicate 6-NHL repeat proteins. Protein locations shown are based on P-sort predictions. Numbers above genes indicate the number of CxxCH motifs predicted to bind cytochrome *c*. IM: inner membrane; OM: outer membrane. For more details, see Table 1 and Table S3.

About 0.2 mM of NH_4^+ would supply 1.6 mM electron equivalents, which is more than enough to account for the observed reduction of 600 μM of Mn(III). This process could operate cryptically if the oxidized products were reduced to N_2 via denitrification enzymes, such as nitrous oxide reductase (cNosZ), which was one of the most abundant proteins expressed in Mn(III)-reducing cultures (Fig. 2c, Table 1).

Carbon metabolism

'Ca. D. occultata' appeared to be growing mixotrophically. 'Ca. *D. occultata*' encoded several central metabolic pathways, including a complete TCA cycle with a glyoxylate bypass, an incomplete (acetate-dependent) 3-hydroxypropionate bicycle, a modified Calvin–Benson–Bassham (CBB) pathway and a pathway for synthesis of polyhydroxybutyrate (Fig. S9). In addition, 'Ca. *D. occultata*' encoded genes for organic carbon transport, and lactate, acetate, and propionate utilization (Fig. S10). Like *D. agitata* and *D. denitrificans*, the CBB pathway of 'Ca. D. occultata' did not encode RuBisCO and sedoheptulose-1,7-bisphosphatase (SHbisPase; Fig. S10); SHbisPase may be replaced by 6-phosphofructokinase and an energy-generating pyrophosphatase (RIX41248; Kleiner *et al.*, 2012; Zorz *et al.*, 2018). The presence of incomplete carbon fixation pathways and organic carbon utilization pathways suggests that 'Ca. *D. occultata*' relies on organic carbon to fix inorganic carbon mixotrophically. The source of this organic carbon could have been ethanol, which is converted to acetate via the pathway discussed in the previous section.

Effect of methane

Although we did not measure appreciable $^{13}CH_4$ oxidation to $^{13}CO_2$, CH_4 stimulated Mn(III) reduction and cytochrome expression in '*Ca*. D. occultata' enrichment cultures. While the specific role of CH_4 in Mn(III) reduction remains unknown, the addition of CH_4 appeared to significantly stimulate expression of many cytochrome *c* proteins, including OccABGJK, MtoD-2 and cytochrome-*c*4 and -*c*5 proteins associated with anaerobic respiration ($p < 0.05$; Table 1-). Expression of several '*Ca*. D. occultata' proteins involved in outer membrane structure and composition—including an extracellular DUF4214 protein located next to an S-layer protein similar to those involved in manganese binding and deposition (Wang *et al.*, 2009), a serine protease possibly involved in Fe(III) particle attachment (Burns *et al.*, 2009), an extracellular PEP-CTERM sorting protein for protein export (Haft *et al.*, 2006) and a Tol-Pal system for outer membrane integrity—was higher in the presence of CH_4 (Table 1).

Transporters and sensors

Numerous transporters were present in the '*Ca*. D. occultata' genome, including 26 TonB-dependent siderophore transporters, 13 TRAP transporters for dicarboxylate transport, as well as ABC transporters for branched-chained amino acids and dipeptides and polypeptides (Table S4). '*Ca*. D. occultata' also contained a large number of environmental sensing genes: 52 bacterial haemoglobins with PAS-PAC sensors, eight TonB-dependent receptors and eight NO responsive regulators (Dnr: Crp/fr family; Table S4). Uniquely in '*Ca*. D. occultata', PAC-PAS sensors flanked accessory genes *nosFLY* on the *c-nosZ* operon (Fig. S7). Comparison of these flanking PAC-PAS sensors in '*Ca*. D. occultata' with O_2-binding sensors revealed that an arginine ~20 aa upstream from the conserved histidine as the distal pocket ligand for O_2-binding is not present in either sensor (Fig. S11), suggesting that the sensor may bind a different ligand, possibly NO, consistent with the placement of these genes next to cNosZ (Shimizu *et al.*, 2015).

Nutrient storage

Active synthesis of storage polymers suggested that '*Ca*. D. occultata' was experiencing electron acceptor starvation at the time of harvesting, consistent with Mn(III) depletion in the bottles (Liu *et al.*, 2015; Guanghuan *et al.*, 2018). Polyphosphate-related proteins, including phosphate transporters, polyphosphate kinase, polyphosphatase and poly-3-hydroxybutyrate synthesis machinery were detected in the proteome (Table S4). Polyphosphate-accumulating organisms store polyphosphates with energy generated from organic carbon oxidation during aerobic respiration or denitrification. These stored compounds are later hydrolyzed when respiratory electron acceptors for ATP production are limiting. Cyanophycin was actively synthesized for nitrogen storage.

Geobacter

'*Ca*. Geobacter occultata' expressed proteins in the TCA cycle at moderate abundance. '*Ca*. G. occultata' contained 17 multiheme c-type cytochromes, none of which were detected in the proteome. The lack of expression of electron transport and metal-reducing pathways makes it unlikely that '*Ca*. G. occultata' was solely responsible for Mn(III) reduction observed in the incubations. A periplasmic group I Ni-Fe hydrogenase (RNC64340; 91% identity to a protein (RLB64899) from *Geobacter* MAG from terrestrial hot spring sediment) and a type IV pilin (RNC67631; 10% aromatics, 87% identity to *Geobacter*

pickeringii (Holmes *et al*., 2016)) were significantly more expressed in the presence of CH_4 than N_2 in the '*Ca*. G. occultata' proteome ($p < 0.05$; Table 1). It is possible that '*Ca*. G. occultata' transferred electrons to '*Ca*. D. occultata' via e-pilins (e.g. direct interspecies electron transfer), contributing to the higher rates of Mn(III) reduction in the presence of CH_4 vs. N_2. The possible involvement of *Geobacter* e-pilins in Mn(III) reduction remains an open question, due to the lack of studies examining the possibility of Mn(III) reduction in *Deltaproteobacteria*.

Conclusions

To our knowledge, this study provides the first evidence for the biological reduction of soluble Mn(III) by a bacterium outside of the *Gammaproteobacteria* class. The dominant bacterium in Mn(III)-reducing enrichment cultures was '*Ca*. D. occultata', a member of the *Rhodocyclales* order of *Betaproteobacteria*. '*Ca*. D. occultata' expressed decahemes similar to the Mto pathway, and *occ* genes, including a novel extracellular undecaheme (OccP), which are predicted to encode a new respiratory electron transport pathway. The novel *occ* operon was found to be widespread in *Betaproteobacteria* from the deep subsurface, where metal cycling can fuel microbial metabolism. We also found highly expressed peptides from various central metabolic cycles and organic substrate utilization pathways, suggesting that '*Ca*. *D. occultata*' may have been using multiple pathways simultaneously for energy generation and carbon assimilation during Mn(III) reduction.

Puzzles remain about whether '*Ca*. D. occultata' can transform two potent greenhouse gases: methane and nitrous oxide. Although '*Ca*. D. occultata' was enriched with CH_4 as the sole electron donor and cultures reduced Mn(III) more rapidly in the presence of CH_4, no CH_4 oxidation activity was measured in Mn(III)-reducing cultures, and proteomic data suggested that '*Ca*. D. occultata' was growing mixotrophically rather than assimilating CH_4. Furthermore, although we did not add oxidized nitrogen compounds to our media, and Mn(III) did not chemically oxidize NH_4^+ under our culture conditions, type II nitrous oxide reductase (cNosZ) was one of the most abundant proteins expressed in Mn(III)-reducing cultures. The role of cNosZ and other denitrification enzymes in '*Ca*. D. occultata' metabolism, and their possible connection to Mn(III) reduction, remain to be investigated.

Acknowledgements

References

Aigle, A., Bonin, P., Iobbi-Nivol, C., Mejean, V., and Michotey, V. (2017) Physiological and transcriptional approaches reveal connection between nitrogen and manganese cycles in Shewanella algae C6G3. *Sci Rep* **7**: 44725.

Anantharaman, K., Brown, C.T., Hug, L.A., Sharon, I., Castelle, C.J., Probst, A.J., *et al*. (2016) Thousands of microbial genomes shed light on interconnected biogeochemical processes in an aquifer system. *Nat Commun* **7**: 13219.

Beal, E.J., House, C.H., and Orphan, V.J. (2009) Manganese- and iron-dependent marine methane oxidation. *Science* **325**: 184–187.

Blomberg, M.R., and Siegbahn, P.E. (2014) Proton pumping in cytochrome c oxidase: energetic requirements and the role of two proton channels. *Biochim Biophys Acta* **1837**: 1165–1177.

Boumaiza, H., Coustel, R., Despas, C., Ruby, C., and Bergaoui, L. (2018) Interaction of ammonium with birnessite: evidence of a chemical and structural transformation in alkaline aqueous medium. *J Solid State Chem* **258**: 543–550.

Brown, D.G., Komlos, J., and Jaffé, P.R. (2005) Simultaneous utilization of acetate and hydrogen by Geobacter sulfurreducens and implications for use of hydrogen as an indicator of redox conditions. *Environ Sci Technol* **39**: 3069–3076.

Burns, J.L., Ginn, B.R., Bates, D.J., Dublin, S.N., Taylor, J. V., Apkarian, R.P., *et al*. (2009) Outer membrane-associated serine protease involved in adhesion of *Shewanella oneidensis* to Fe(III) oxides. *Environ Sci Technol* **44**: 68–73.

Chen, J., and Strous, M. (2013) Denitrification and aerobic respiration, hybrid electron transport chains and co-evolution. *Biochimica et Biophysica Acta (BBA)-Bioenergetics* **1827**: 136–144.

Crowe, S.A., Canfield, D.E., Mucci, A., Sundby, B., and Maranger, R. (2012) Anammox, denitrification and fixed-nitrogen removal in sediments from the lower St. Lawrence Estuary. *Biogeosciences* **9**: 4309–4321.

Crowe, S.A., Katsev, S., Leslie, K., Sturm, A., Magen, C., Nomosatryo, S., *et al*. (2011) The methane cycle in ferruginous Lake Matano. *Geobiology* **9**: 61–78.

Crowe, S.A., O'Neill, A.H., Katsev, S., Hehanussa, P., Haffner, G.D., Sundby, B., *et al*. (2008) The biogeochemistry of tropical lakes: a case study from Lake Matano, Indonesia. *Limnol Oceanogr* **53**: 319–331.

Cummings, D.E., Caccavo, F., Spring, S., and Rosenzweig, R.F. (1999) Ferribacterium limneticum, gen. nov., sp. nov., an Fe(III)-reducing microorganism isolated

from mining-impacted freshwater lake sediments. *Arch Microbiol* **171**: 183–188.

Diem, D., and Stumm, W. (1984) Is dissolved Mn^{2+} being oxidized by O_2 in absence of Mn-bacteria or surface catalysts? *Geochim Cosmochim Acta* **48**: 1571–1573.

Edwards, M.J., Hall, A., Shi, L., Fredrickson, J.K., Zachara, J.M., Butt, J.N., et al. (2012) The crystal structure of the extracellular 11-heme cytochrome UndA reveals a conserved 10-heme motif and defined binding site for soluble iron chelates. *Structure* **20**: 1275–1284.

Emerson, D., Field, E.K., Chertkov, O., Davenport, K.W., Goodwin, L., Munk, C., et al. (2013) Comparative genomics of freshwater Fe-oxidizing bacteria: implications for physiology, ecology, and systematics. *Front Microbiol* **4**: 254.

Ettwig, K.F., Zhu, B., Speth, D., Keltjens, J.T., Jetten, M.S. M., and Kartal, B. (2016) Archaea catalyze iron-dependent anaerobic oxidation of methane. *Proc Natl Acad Sci U S A* **113**: 12792–12796.

Finneran, K.T., Johnsen, C.V., and Lovley, D.R. (2003) *Rhodoferax ferrireducens* sp. nov., a psychrotolerant, facultatively anaerobic bacterium that oxidizes acetate with the reduction of Fe(III). *Int J Syst Evol Microbiol* **53**: 669–673.

Fredrickson, J.K., Romine, M.F., Beliaev, A.S., Auchtung, J. M., Driscoll, M.E., Gardner, T.S., et al. (2008) Towards environmental systems biology of *Shewanella*. *Nat Rev Microbiol* **6**: 592–603.

Gonska, N., Young, D., Yuki, R., Okamoto, T., Hisano, T., Antonyuk, S., et al. (2018) Characterization of the quinol-dependent nitric oxide reductase from the pathogen *Neisseria meningitidis*, an electrogenic enzyme. *Sci Rep* **8**: 3637.

Guanghuan, G., Jianqiang, Z., Aixia, C., Bo, H., Ying, C., Kun, G., et al. (2018) Nitrogen removal and nitrous oxide emission in an anaerobic/oxic/anoxic sequencing biofilm batch reactor. *Environ Eng Sci* **35**: 19–26.

Haft, D.H., Paulsen, I.T., Ward, N., and Selengut, J.D. (2006) Exopolysaccharide-associated protein sorting in environmental organisms: the PEP-CTERM/EpsH system. Application of a novel phylogenetic profiling heuristic. *BMC Biol* **4**: 29.

He, S., Barco, R.A., Emerson, D., and Roden, E.E. (2017) Comparative genomic analysis of neutrophilic iron(II) oxidizer genomes for candidate genes in extracellular electron transfer. *Front Microbiol* **8**: 1584.

Heintze, S., and Mann, P. (1947) Soluble complexes of manganic manganese. *J Agric Sci* **37**: 23–26.

Hem, J.D. (1963) *Chemical equilibria and rates of manganese oxidation*, Washington DC: US Government Printing Office.

Hernsdorf, A.W., Amano, Y., Miyakawa, K., Ise, K., Suzuki, Y., Anantharaman, K., et al. (2017) Potential for microbial H_2 and metal transformations associated with novel bacteria and archaea in deep terrestrial subsurface sediments. *ISME J* **11**: 1915–1929.

Holmes, D.E., Dang, Y., Walker, D.J., and Lovley, D.R. (2016) The electrically conductive pili of *Geobacter* species are a recently evolved feature for extracellular electron transfer. *Microb Genom* **2**: e000072.

Ji, B., Yang, K., Zhu, L., Jiang, Y., Wang, H., Zhou, J., and Zhang, H. (2015) Aerobic denitrification: a review of important advances of the last 30 years. *Biotechnology and Bioprocess Engineering* **20**: 643–651.

Jones, C., Crowe, S.A., Sturm, A., Leslie, K.L., MacLean, L. C.W., Katsev, S., et al. (2011) Biogeochemistry of manganese in ferruginous Lake Matano, Indonesia. *Biogeosciences* **8**: 2977–2991.

Jung, H., Taillefert, M., Sun, J., Wang, Q., Borkiewicz, O.J., Liu, P., et al. (2020) Redox cycling driven transformation of layered manganese oxides to tunnel structures. *J Am Chem Soc* **142**: 2506–2513.

Kato, S., Ohkuma, M., Powell, D.H., Krepski, S.T., Oshima, K., Hattori, M., et al. (2015) Comparative genomic insights into ecophysiology of neutrophilic, micro-aerophilic iron oxidizing bacteria. *Front Microbiol* **6**: 1265.

Kleiner, M., Wentrup, C., Lott, C., Teeling, H., Wetzel, S., Young, J., et al. (2012) Metaproteomics of a gutless marine worm and its symbiotic microbial community reveal unusual pathways for carbon and energy use. *Proc Natl Acad Sci U S A* **109**: 1173–1182.

Kostka, J.E., Luther, G.W., and Nealson, K.H. (1995) Chemical and biological reduction of Mn(III)-pyrophosphate complexes - potential importance of dissolved Mn(III) as an environmental oxidant. *Geochim Cosmochim Acta* **59**: 885–894.

Kuntz, L.B., Laakso, T.A., Schrag, D.P., and Crowe, S.A. (2015) Modeling the carbon cycle in Lake Matano. *Geobiology* **13**: 454–461.

Learman, D., Wankel, S., Webb, S., Martinez, N., Madden, A., and Hansel, C. (2011) Coupled biotic–abiotic Mn (II) oxidation pathway mediates the formation and structural evolution of biogenic Mn oxides. *Geochem Cosmochim Acta* **75**: 6048–6063.

Leu, A.O., Cai, C., McIlroy, S.J., Southam, G., Orphan, V.J., Yuan, Z., et al. (2020) Anaerobic methane oxidation coupled to manganese reduction by members of the Methanoperedenaceae. *ISME J* **14**: 1030–1041.

Lin, Y.-C., Sekedat, M.D., Cornell, W.C., Silva, G.M., Okegbe, C., Price-Whelan, A., et al. (2018) Phenazines regulate nap-dependent denitrification in Pseudomonas aeruginosa biofilms. *J Bacteriol* **200**: e00031–e00018.

Liu, Y., Peng, L., Guo, J., Chen, X., Yuan, Z., and Ni, B.-J. (2015) Evaluating the role of microbial internal storage turnover on nitrous oxide accumulation during denitrification. *Sci Rep* **5**: 15138.

Luther, G.W., Thibault de Chanvalon, A., Oldham, V.E., Estes, E.R., Tebo, B.M., and Madison, A.S. (2018) Reduction of manganese oxides: thermodynamic, kinetic and mechanical considerations for one- versus two-electron transfer steps. *Aquatic Geochem* **24**: 257–277.

Luther, G.W., III, Madison, A.S., Mucci, A., Sundby, B., and Oldham, V.E. (2015) A kinetic approach to assess the strengths of ligands bound to soluble Mn (III). *Mar Chem* **173**: 93–99.

Madison, A.S., Tebo, B.M., Mucci, A., Sundby, B., and Luther, G.W., 3rd. (2013) Abundant porewater Mn(III) is a major component of the sedimentary redox system. *Science* **341**: 875–878.

Morgan, J.J. (2005) Kinetics of reaction between O_2 and Mn (II) species in aqueous solutions. *Geochim Cosmochim Acta* **69**: 35–48.

Niemann, H., Steinle, L., Blees, J., Bussmann, I., Treude, T., Krause, S., *et al*. (2015) Toxic effects of lab-grade butyl rubber stoppers on aerobic methane oxidation. *Limnol Oceangr: Methods* **13**: 40–52.

Oldham, V.E., Siebecker, M.G., Jones, M.R., Mucci, A., Tebo, B.M., and Luther, G.W. (2019) The speciation and mobility of Mn and Fe in estuarine sediments. *Aquat Geochem* **25**: 3–26.

Richardson, D.J., Butt, J.N., Fredrickson, J.K., Zachara, J. M., Shi, L., Edwards, M.J., *et al*. (2012) The 'porin–cytochrome' model for microbe-to-mineral electron transfer. *Mol Microbiol* **85**: 201–212.

Riedinger, N., Formolo, M.J., Lyons, T.W., Henkel, S., Beck, A., and Kasten, S. (2014) An inorganic geochemical argument for coupled anaerobic oxidation of methane and iron reduction in marine sediments. *Geobiology* **12**: 172–181.

Shi, L., Belchik, S.M., Wang, Z., Kennedy, D.W., Dohnalkova, A.C., Marshall, M.J., *et al*. (2011) Identification and characterization of UndAHRCR-6, an outer membrane endecaheme c-type cytochrome of *Shewanella* sp. strain HRCR-6. *Appl Environ Microbiol* **77**: 5521–5523.

Shi, L., Dong, H., Reguera, G., Beyenal, H., Lu, A., Liu, J., *et al*. (2016) Extracellular electron transfer mechanisms between microorganisms and minerals. *Nat Rev Microbiol* **14**: 651.

Shimizu, T., Huang, D., Yan, F., Stranava, M., Bartosova, M., Fojtíková, V., and Martínková, M.t. (2015) Gaseous O_2, NO, and CO in signal transduction: structure and function relationships of heme-based gas sensors and heme-redox sensors. *Chem Rev* **115**: 6491–6533.

Smith, J.A., Lovley, D.R., and Tremblay, P.L. (2013) Outer cell surface components essential for Fe(III) oxide reduction by Geobacter metallireducens. *Appl Environ Microbiol* **79**: 901–907.

Spiro, S. (2012) Nitrous oxide production and consumption: regulation of gene expression by gas-sensitive transcription factors. *Philos Trans R Soc Lond B Biol Sci* **367**: 1213–1225.

Sturm, A., Fowle, D.A., Jones, C., Leslie, K., Nomosatryo, S., Henny, C., *et al*. (2019) Rates and pathways of CH_4 oxidation in ferruginous Lake Matano, Indonesia. *Geobiology* **17**: 294–307.

Szeinbaum, N., Burns, J.L., and DiChristina, T.J. (2014) Electron transport and protein secretion pathways involved in Mn(III) reduction by Shewanella oneidensis. *Environ Microbiol Rep* **6**: 490–500.

Szeinbaum, N., Lin, H., Brandes, J.A., Taillefert, M., Glass, J.B., and DiChristina, T.J. (2017) Microbial manganese(III) reduction fuelled by anaerobic acetate oxidation. *Environ Microbiol* **19**: 3475–3486.

Tebo, B.M., Johnson, H.A., McCarthy, J.K., and Templeton, A.S. (2005) Geomicrobiology of manganese(II) oxidation. *Trends Microbiol* **13**: 421–428.

Wang, X., Schröder, H.C., Schloßmacher, U., and Müller, W. E. (2009) Organized bacterial assemblies in manganese nodules: evidence for a role of S-layers in metal deposition. *Geo-Mar Lett* **29**: 85–91.

Wegener, G., Niemann, H., Elvert, M., Hinrichs, K.U., and Boetius, A. (2008) Assimilation of methane and inorganic carbon by microbial communities mediating the anaerobic oxidation of methane. *Environ Microbiol* **10**: 2287–2298.

Yamaguchi, K.S., and Sawyer, D.T. (1985) The redox chemistry of manganese(III) and manganese(IV) complexes. *Isr J Chem* **25**: 164–176.

Yang, Y., Chen, J., Qiu, D., and Zhou, J. (2013) Roles of UndA and MtrC of *Shewanella putrefaciens* W3-18-1 in iron reduction. *BMC Microbiol* **13**: 267.

Yu, H., and Leadbetter, J.R. (2020). Bacterial chemolithoautotrophy via manganese oxidation. *Nature*, **583**, (7816), 453–458. http://dx.doi.org/10.1038/s41586-020-2468-5.

Zorz, J.K., Kozlowski, J.A., Stein, L.Y., Strous, M., and Kleiner, M. (2018) Comparative proteomics of three species of ammonia-oxidizing bacteria. *Front Microbiol* **9**: 938.

Supporting Information

Additional Supporting Information may be found in the online version of this article at the publisher's web-site:

Appendix S1: Supporting Information
Table S3: Supporting information
Table S4: Supporting information